Acta Oceanol. Sin., 2017, Vol. 36, No. 1, P. 35–43
DOI: 10.1007/s13131-016-0883-0
http://www.hyxb.org.cn
E-mail: hyxbe@263.net

Regime shift of the dominant factor for halocline depth in the Canada Basin during 1990–2008

MU Longjiang[1]*, ZHAO Jinping[1], ZHONG Wenli[1]

[1] Physical Oceanography Laboratory, Ocean University of China, Qingdao 266100, China

Received 6 January 2016; accepted 2 March 2016

Abstract

The World Ocean Database (WOD) is used to evaluate the halocline depth simulated by an ice-ocean coupled model in the Canada Basin during 1990–2008. Statistical results show that the simulated halocline is reliable. Comparing of the September sea ice extent between simulation and SSM/I dataset, a consistent interannual variability is found between them. Moreover, both the simulated and observed September sea ice extent show staircase declines in 2000–2008 compared to 1990–1999. That supports that the abrupt variations of the ocean surface stress curl anomaly in 2000–2008 are caused by rapid sea ice melting and also in favor of the realistic existence of the simulated variations. Responses to these changes can be found in the upper ocean circulation and the intermediate current variations in these two phases as well. The analysis shows that seasonal variations of the halocline are regulated by the seasonal variations of the Ekman pumping. On interannual time scale, the variations of the halocline have an inverse relationship with the ocean surface stress curl anomaly after 2000, while this relationship no longer applies in the 1990s. It is pointed out that the regime shift in the Canada Basin can be derived to illustrate this phenomenon. Specifically, the halocline variations are dominated by advection in the 1990s and Ekman pumping in the 2000s respectively. Furthermore, the regime shift is caused by changing Transpolar Drift pathway and Ekman pumping area due to spatial deformation of the center Beaufort high (BH) relative to climatology.

Key words: Canada Basin, Beaufort high, Transpolar Drift, circumpolar boundary current, halocline depth, freshwater

Citation: Mu Longjiang, Zhao Jinping, Zhong Wenli. 2017. Regime shift of the dominant factor for halocline depth in the Canada Basin during 1990–2008. Acta Oceanologica Sinica, 36(1): 35–43, doi: 10.1007/s13131-016-0883-0

1 Introduction

The freshwater mixed by summer ice melt water, river runoff, precipitation and the Pacific water widely covers the upper ocean in the Canada Basin. The summer Pacific water (T>–1.0°C, 31<S<33) and the winter Pacific water (S=33.1) occupy a depth range between 50 and 150 m. In the intermediate layer, the Atlantic water (AW) with the core layer's salinity higher than 34.5 and temperature higher than 0°C occupies a depth range between 200 and 1 000 m. Between the Pacific water and the Atlantic water, a permanent halocline dominates the variations of the freshwater and other oceanic processes. Below the AW, the renewal of the Arctic Bottom water with the highest salinity is very slow through the processes of advection and diffusion.

The study area in this paper covers in 69°–78°N, 124°–162°W in the Canada Basin (Fig. 1). A long-term mean sea level pressure (SLP) in Fig. 1 displays the Beaufort high (BH) across eastern Siberia and the Canadian Archipelago with an elliptical shape distribution. As a high pressure center in the central Canada Basin, the generated Beaufort Gyre (BG) controls sea ice drift in the upper layer and tracers (heat and salt) balance of the Arctic. Meanwhile, the low pressure like a wedge from the Nordic Seas into the Arctic interacts with the BH center forming almost parallel isobars to drive the Transpolar Drift.

Recent research suggests that the spin of BG is accelerating and the freshwater content in the Canada Basin is increasing (McPhee et al., 2009; Proshutinsky et al., 2009; Giles et al., 2012), at the same time the summer sea ice extent is decreasing. Observations capture the anomalous warm Atlantic water entering into the Canada Basin and warming the intermediate layer (Shimada et al., 2004). The depth of halocline, the upper layer anticyclonic circulation and the intermediate layer circumpolar current have changed correspondingly in this scenarios. In addition to the general consideration that the BG dominates the halocline's variations, Spall (2013) proposed another mechanism that the depth of halocline is a consequence of the process that the vertical diffusion of salt in the ocean interior to be balanced by eddy transports between boundary current and ocean interior. In summary, the baroclinic processes regulate the bowl-shaped halocline in the Canada Basin. Accordingly, the freshwater in the upper layer is the major factor to maintain the present observations of the circulation patterns and halocline distributions. Lique et al. (2015) shared the same point of view with Spall (2013) from an ideal Arctic model. In addition, she pointed out that the change of the upper circulation can significantly affect the intermediate current, but the enhanced intermediate inflow cannot alter the upper layer circulation obviously.

Although the results of ideal models motivate a lot on the comprehension of the oceanic processes in the Canada Basin,

Foundation item: The National Basic Research Program (973 Program) of China under contract No. 2015CB953900; the National Natural Science Foundation of China under contract No. 41330960.
*Corresponding author, E-mail: oucmlj@gmail.com

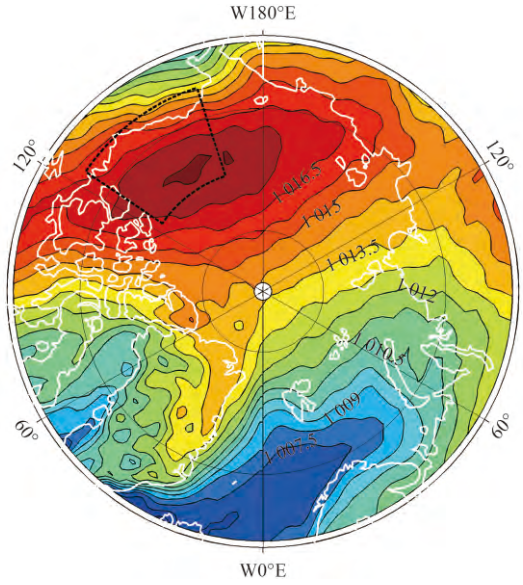

Fig. 1. Long-term mean sea level pressure (SLP) of 1979–2010 in the Arctic with the study area indicated by dashed frame. The SLP data is derived from JRA-25 with contour labels shown in hPa.

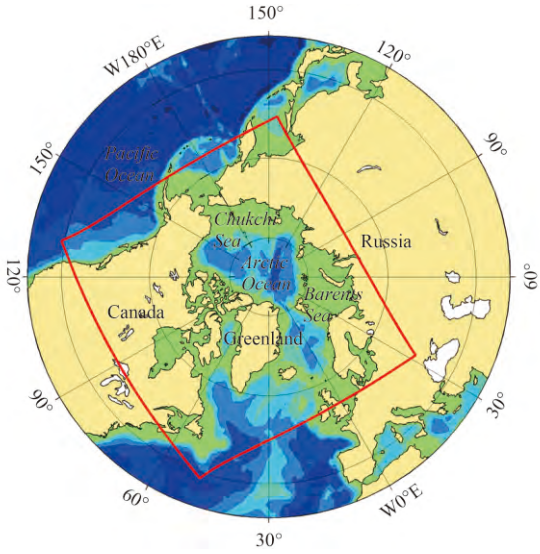

Fig. 2. The arctic regional model domain (red square).

time variations of these processes remain unknown. The oceanic processes in the Canada Basin always show seasonal, interannual and decadal variabilities modulated by atmospheric circulations. In this paper, we use an ice-ocean coupled model to simulate the variations of the halocline, the freshwater content, the upper layer circulation and the intermediate layer current from 1990 to 2008 in the Canada Basin, then investigate the controlling factors of the halocline distributions. The paper is arranged as follows: the ice-ocean coupled model configuration and data used for validation are described in Section 2; an evaluation the between simulation and the observation is present in Section 3; time series of the halocline, the freshwater, the upper layer circulation and the intermediate layer current in the Canada Basin are shown in Section 4; the mechanism that controls the halocline distribution is discussed in Section 5.

2 Model and datasets

We use a regional ice-ocean coupled model based on Massachusetts Institute of Technology general circulation model (MITgcm) (Marshall et al., 1997). The model configuration is identical to that of Losch et al. (2010), and Heimbach et al. (2010) with some parameters optimized by Nguyen et al. (2011). The model domain is demonstrated in Fig. 2.

The ocean component of the model using an orthogonal curvilinear coordinate in one of six cube spheres (Adcroft et al., 2004) can effectively avoid the computational instability due to an extreme small time step around the North Pole. There are 50 layers in the vertical with 20 layers above 300 m to resolve the halocline and slowly increasing to 450 m each layer below 300 m. An equation of ocean state formulated according to Jackett and McDougall (1995) is used. The momentum equations in vector invariant form are discretized on Arakawa C grid and integrated by the finite volume method. The slip lateral boundaries and no-slip bottom with a quadratic drag coefficient are applied. The horizontal viscosity coefficients are computed by biharmonic Smagorinsky scheme. To improve computational stability, vertical viscosity and diffusion terms are treated implicitly. The KPP (Large et al., 1994) closure scheme is chosen to parameterize boundary layer and convection. Besides, a latitude dependent enhanced background tracer diffusion ranges from 10^{-7} to 10^{-5} m^2/s is used to represent unresolved eddy mixing. The model employs a 7th-order monotonicity preserving advection scheme (Daru and Tenaud, 2004) and a zero explicit horizontal diffusivity for weak diffusion in the Arctic Ocean interior. Ocean surface fluxes are calculated by bulk formula (Large and Pond, 1982). The sea ice component is set on the same grid with viscous-plastic (VP) model (Hibler, 1979) in ice dynamics and zero-layer model in thermodynamics. According to dry and wet conditions, the sea ice albedos are set to 0.70 and 0.65, and the snow albedos are set to 0.80 and 0.75.

Bathymetry is derived from the International Bathymetric Chart of the Arctic Ocean (IBCAO) product. For initial conditions, temperature and salinity fields are interpolated by PHC 3.0 datasets, sea ice fields are interpolated by datasets from Pan-Arctic Ice-Ocean Modeling and Assimilation System (Zhang and Rothrock, 2003). The model is forced by Japanese 25-year Reanalysis Project (JRA25) (Onogi et al., 2007) with radiative fluxes from Climate Forecast System Reanalysis (CFSR). The open boundary fields are interpolated from ECCO2 datasets (Nguyen et al., 2011) and the climatology Arctic runoff database is used (Lammers et al., 2001; Shiklomanov et al., 2000). More important, the model incorporates no temperature or salinity relaxing scheme. The model starts from 1980 and has been integrated for about 30 a. The regional model reaches equilibrium in 10 a due to fast adjustment. And model results in 1990–2008 are used for analysis.

In addition, data from World Ocean Database (WOD) is used for model evaluation. The ice concentration data from Special Sensor Microwave Imager (SSM/I) and the sea ice drift data from Polar Pathfinder monthly 25 km EASE-Grid Sea Ice Motion Vectors are obtained from the National Snow and Ice Data Center (NSIDC).

3 Model evaluation

Before 2002, most CTD profiles were deployed on the peripheral of the Canada Basin. After that, with the employment of ITPs and more CTD stations, we could now have a clearer spatial pattern of the thermohaline structure.

The salinity of the Fram Strait Branch (FSB) of the Atlantic inflow is above 34.5. The other branch (the Barents Sea Branch) of the Atlantic inflow loses heat in the Barents Sea and subducts into the Arctic basin through St. Anna Trough below the FSB (Rudels et al., 1999, 2000). We use a similar maximum angle method as suggested by Chu and Fan (2011) to determine the halocline depth where the salinity greater than 34.5 exists in the water column. Because the halocline has a seasonal variation in the Canada Basin (Proshutinsky et al., 2009), the CTD stations deployed in summer cannot fully capture the annual mean state. Nevertheless, the halocline depth derived from the CTD and picked-up ITP profiles represents the spatial distribution roughly and is compared with the simulated results. Compared to observations in 1990–2008 (Fig. 3), the ice-ocean coupled model reproduced reasonable spatial distribution and temporal variations of the halocline depth. Owing to the dominating anticyclonic circulation in the Canada Basin, both observations and simulation present a bowl-shaped halocline spatial distribution. In the basin interior, Ekman pumping deepens the halocline. While along the continental slope, horizontal Ekman transport requires a vertical compensation which raises the halocline at the same time. Both observations and simulation show that the halocline has been undergoing a basin scale uniformly deepening or shallowing in some years, such as the shallowing of the halocline in the whole basin in 2003 and deepening in 2008. Particularly, the halocline near the Chukchi Sea shows more interannual variabilities than other regions.

Figure 4 shows that the mean absolute deviation of the whole basin between the observations and the simulation is about 30 m. The deviations change dramatically before 2002, but start to

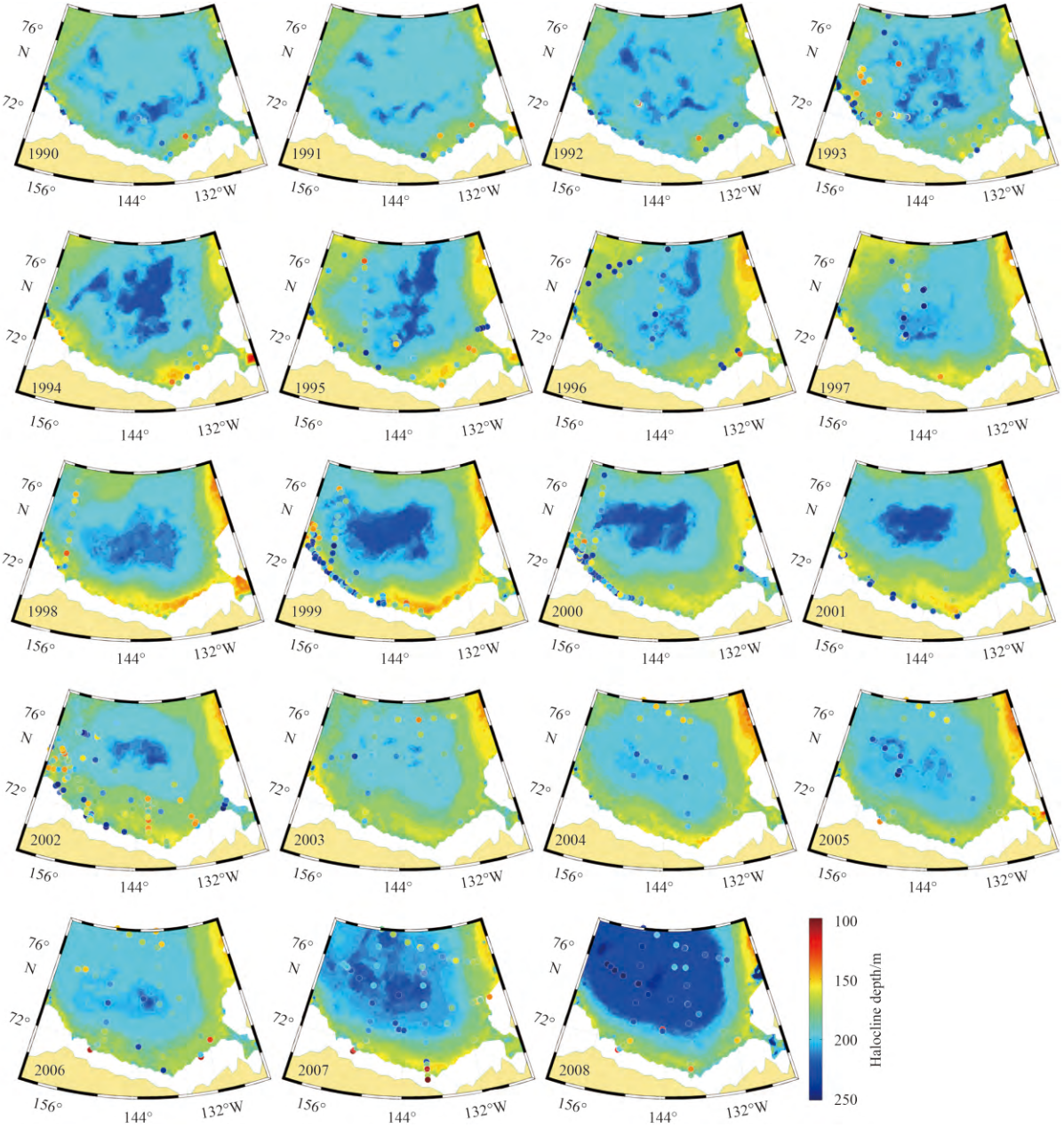

Fig. 3. Simulated annual mean depth of the halocline in the Canada Basin (shading) and observed values calculated from WOD (color dots).

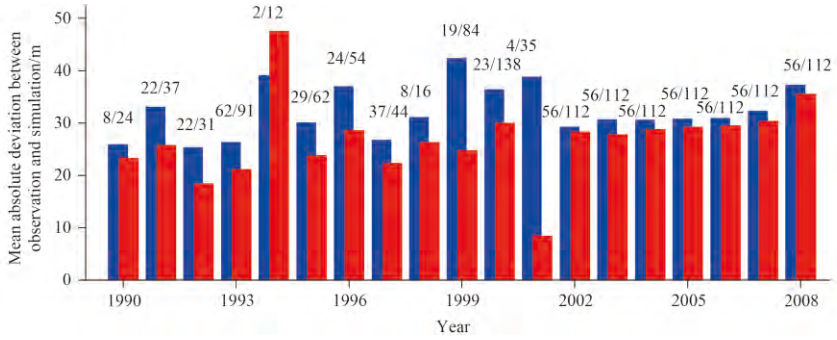

Fig. 4. The mean absolute deviation between observation and simulation of the sampled stations. The red bars represent the mean absolute deviations of the basin interior, while the blue bars represent those of the whole basin. The numbers on the top of the bars (such as 8/24) indicate the stations in the interior (8) and the whole basin (24).

change little after that time when more data observed. The mean vertical grid spacing in the model is about 18.3 m where halocline is located. Such that the mean absolute deviation above is no more than two grids, that indicating a reliable simulated halocline. The mean absolute deviations of the basin interior (red bars in Fig. 4) are below the whole basin mean (blue bars in Fig. 4) except in 1994 with only two samples in the ocean interior. That is to say, the absolute deviations near the continental slope are higher than those of the basin interior, thus cause most biases. The horizontal Ekman transport modulated by the synoptic scale wind significantly, that is responsible for the larger biases of the halocline along the continental slope between the observations and the simulation as seen from Fig. 3. On the basis of the comparison and statistics analysis above, we believe that the simulation shows resemblances to realistic situation somehow.

4 Simulated variations in the Canada Basin

4.1 *Variations of the ocean surface stress curl*

The BH is the main factor to control ocean dynamics in the Canada Basin and that can be reflected by ocean surface stress curl. The ocean surface stress curl is model output calculated on the interface between atmosphere and ocean when there is no ice, or on the interface between ice and ocean when ice covers. The positive anomaly of the red time series in Fig. 5 indicates weakening of the anticyclonic BG and the negative anomaly indicates strengthening of the BG respectively. Besides deseasonalizing variations, interannual variations are also pronounced. We can see that the positive and negative phase transitions occurred during 1990–2008 in the Canada Basin. Compared to the 1990s, the ocean surface stress curl changes with nearly two times enhanced amplitude variations.

Sea ice absorbs energy that wind exerts on the ocean. With decreasing of ice concentration and thinning of ice thickness, less wind energy is dissipated by the sea ice, thus more energy can be imposed on the ocean surface. In Fig. 6, we compare the September sea ice extent calculated from model results and the sea ice concentration datasets from SSM/I. The variabilities of the sea ice extent in the model appear consistent with those in the SSM/I, although with some acceptable biases. The mean ice extent in 1990–1999 derived from the SSM/I is 7.20×10^5 km^2, while decreases to 5.42×10^5 km^2 abruptly in 2000–2008 like a staircase. The same staircase is also found in the model results, which from 5.95×10^5 km^2 down to 4.88×10^5 km^2. Sensitivity cases in Yang (2009) also highlight the increased energy into the ocean due to rapid sea ice melting in the Arctic. What discussed above illustrates the abrupt amplitude change of the ocean surface curl anomaly.

4.2 *Variations of the freshwater content and the halocline depth*

The liquid freshwater content (LFWC, c_{lfw}) in the Canada Basin is calculated as follows:

$$c_{\mathrm{lfw}} = \int_{\Omega} \mathrm{d}A \int_{h(S_{\mathrm{ref}})}^{0} \left(1 - S\left(z\right)/S_{\mathrm{ref}}\right) \mathrm{d}z,$$

where S is the insitu salinity, S_{ref} $(= 34.8)$ is the reference salinity (Aagaard and Carmack, 1989; Carmack, 2000; Carmack et al.,

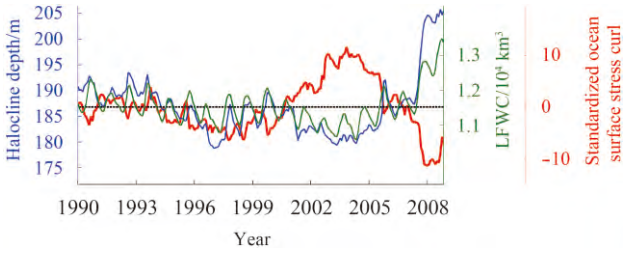

Fig. 5. Variations of halocline depth (blue), LFWC (green) and ocean surface stress curl (red). The dash line indicates the mean for all three time series. The ocean surface stress curl has been smoothed using 2 a time window to remove seasonal variabilities.

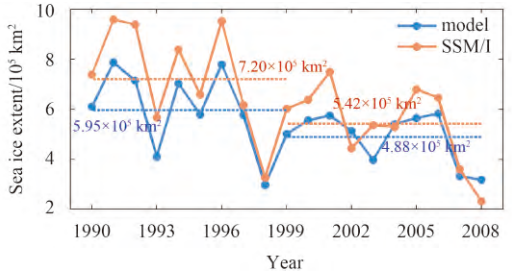

Fig. 6. The September sea ice extent in the Canada Basin. Model results are represented by light blue line. SSM/I data is represented by orange line. The mean values averaged in 1990–1999 and 2000–2008 are represented by dashed lines in different colors respectively.

2008), $h(S_{\mathrm{ref}})$ is the depth of the reference salinity, and Ω is the area of the whole Canada Basin. The reference depth $h(S_{\mathrm{ref}})$ reflects the halocline variabilities to some extent, thus high correlations are found between the time series of halocline (blue in Fig. 5) and freshwater content (green in Fig. 5).

The simulated results suggest that both the freshwater content and the halocline depth are increasing from 1990 to 2008. Before 2003, the Canada Basin experiences the decreasing of the freshwater content in the early 1990s, then the increasing in the late 1990s and the decreasing till 2002. The halocline varies respectively at the same time. Particularly, after 2003, in the rapid warm phase of the Arctic, the rapid increase of the freshwater content and the deepening of halocline are revealed from the model and demonstrated in Fig. 5. Observations from 1992 to 2012 show that the freshwater content in Arctic was increasing with a trend about (600±300) km^3 (Giles et al., 2012), that supports the model results. Changes of the interface between the Atlantic water and the Pacific water from August 2002 to August 2003 observed by a mooring array deployed in 152°W (Fig. 13 in Nikolopoulos et al. (2009)) are identical to our model results in this time span.

Seasonal and interannual variabilities are found in the time series of the halocline depth and the LWFC. In the seasonal scale, there is a significant inverse relationship between the halocline depth and the ocean surface stress curl anomaly. Salt rejected processes during sea ice formation and sea ice melting in summer can also generate the seasonal variations. According to the wind driven circulation theory, a positive (negative) BG anomaly reduces (enhances) the intensity of ocean surface stress curl, thus reduces (enhances) the Ekman pumping and raises (depresses) the halocline. Both observations and simulations demonstrate the evidences of negative relations between changes of freshwater content and ocean surface stress curl (Proshutinsky et al., 2009; Stewart and Haine, 2013; Condron, 2009). Although significant relations discussed above appear after 2000 in Fig. 5, that cannot be satisfied all the time especially between 1994 and 2000 on an interannual time scale. The negative ocean surface stress curl anomaly does not deepen the halocline, but raise on the contrary (Fig. 5). That implies the factors influencing halocline variations in the Canada Basin are more than ocean surface stress curl.

4.3 *Variations of the upper ocean circulation*

We adopt vorticity which is used by Karcher et al. (2012) as a useful scalar to measure the direction and intensity of the upper layer circulations. The basin-scale mean vorticity is calculated as

$$\zeta = \frac{1}{\Omega}\int_{\Omega} \mathrm{d}A \int_{h}^{0} \left(\frac{\partial v}{\partial x} - \frac{\partial u}{\partial y}\right) \mathrm{d}z,$$

where u and v are horizontal components of the velocity and h is the halocline depth. More negative ζ value indicates a stronger BG.

The simulation shows that an anticyclonic circulation pattern ($\zeta < 0$) dominates the Canada Basin with significant interseasonal, seasonal and interannual variations (Fig. 7). The deseasonalizing time series (blue line in Fig. 7) exhibit a strengthening of the anticyclonic upper layer circulation from 1990 to 1998, then weakening from 1999 to 2003. Although lacking of long term current meters observations, the model results in Karcher et al. (2012, Fig. 13) support our simulation.

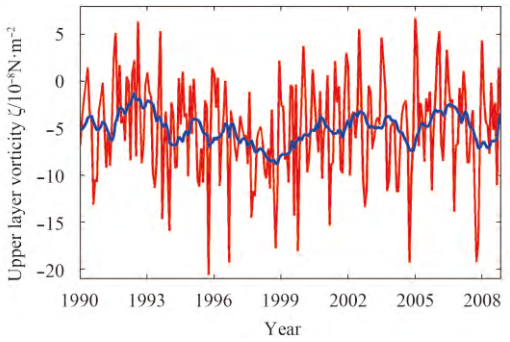

Fig. 7. The upper layer vorticity ζ (red line). The blue line is the deseasonalizing time series using 12 months' time window.

4.4 *Variations of the intermediate ocean current*

The conservation of potential vorticity restricts the circumpolar boundary current to flow along isobaths, thus the current is fast along the continental slope and slow in the basin interior. Considering that, the topostrophy (Holloway, 2008; Zhang and Steele, 2007) can be defined to evaluate the intermediate layer current. As Zhang and Steel (2007), the topostrophy integrated through the basin is

$$\tau = \int_{\Omega} \mathrm{d}A \int_{-H}^{h} \vec{f} \times \vec{V} \cdot \nabla D \mathrm{d}z,$$

where $\vec{f}$ is the Coriolis parameter, $\vec{V}$ is velocity vector, H=1 000 m is the lower bound for integrating, h is the halocline depth, and ∇D is the gradient of the total depth. τ being greater than 0 demonstrates that the shallower water is on the right hand if travelling along the intermediate current. Given the topography of the Canada Basin, currents flow counterclockwise when the topography greater than 0 and clockwise when less than 0. Meanwhile, the magnitude of τ represents its intensity.

The simulation indicates that the counterclockwise intermediate current occupies more than 85.0% of the time during 1990–2008 in the Canada Basin. In some years, the current flows clockwise which has been reported in literature (Karcher et al., 2012). Both seasonal and interannual variations can be found from the time series (Fig. 8). But the intensity of the seasonal variations is weaker than that in the upper layer circulation (Fig. 7). A linear least square fitting in Fig. 8 indicates the intermediate current weakening in 1990–1998, then strengthening in 1999–2005 and weakening again in 2006–2008.

The variability of the intermediate current can be tracked by temperature or salinity as an alternative in the absence of observations. The simulation shows a strong intermediate current in

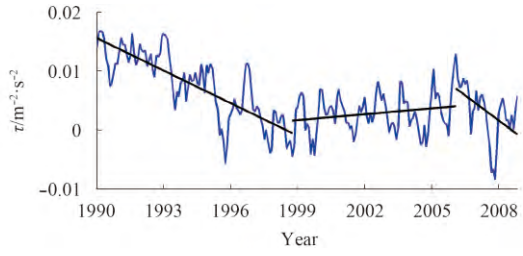

Fig. 8. Topostrophy τ (blue) during 1900–2008. The black lines are the linear least square fitting for three periods.

the earlier 1990s, which is verified by the observed anomaly warmer signal (Shimada et al., 2004; McLaughlin et al., 2009). In some years, the topostrophy τ is less than 0 (Fig. 8) that suggests the existence of anticyclonic current in the intermediate layer. McLaughlin et al. (2009) also reported the existence of anticyclonic currents in 400 m deduced by the gravitational potential relative to 1 000 m when the influence of the Beaufort Gyre is strong.

The standardized vorticity of the upper layer circulation ζ against the standardized topostrophy τ of intermediate layer are plotted in a scatter chart (Fig. 9). The diagram shows a linear relationship between the vorticity and the topography, although with high residuals caused by more seasonal variations embedded in time series of the upper layer circulation than that of intermediate layer. The consistent variations between the two layers in interannual scale can be used to illustrate this phenomenon. When the BG strengthening (the vorticity is decreasing), the intermediate current will weaken respectively (the topography is decreasing) as the influence of the Beaufort Gyre extends into the Atlantic layer. This relationship is also supported using an ideal model by Lique et al. (2015).

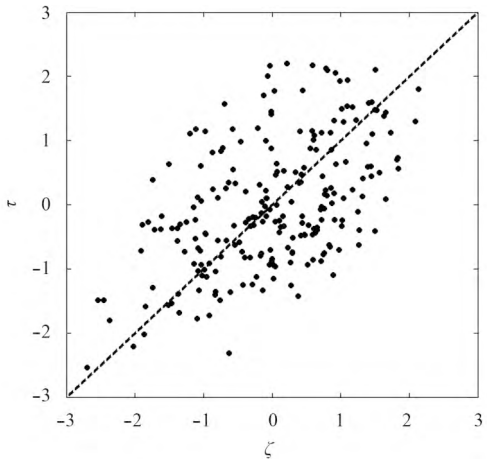

Fig. 9. The standardized vorticity of the upper layer circulation ζ against the standardized topostrophy τ of the intermediate layer.

5 Regime shift of dominant factor for halocline depth

In Section 4.2, we point out that the basin-scale mean halocline depth variations have an inverse relationship with the ocean surface stress curl anomaly after 2000, while the halocline is not deepening but raising on the contrary when a negative ocean surface stress curl anomaly imposed before 2000. That implies a regime shift on control halocline variations in the Canada Basin in the study phase. When the halocline depth changes, the freshwater content, the upper layer circulation and the intermediate layer current will change correspondingly. We try to explore the mechanism that controls the variations in the background.

Considering a simplified ocean column with the halocline depth h on f-plane, the control equation (Cushman-Roisin et al., 2011) of h is

$$\frac{\partial h}{\partial t} = -\frac{\partial uh}{\partial x} - \frac{\partial vh}{\partial y} - w_{\mathrm{E}} + w_{\mathrm{dia}},$$

where w_{E} is Ekman pumping; and w_{dia} is a subduction rate which can be ignored in this situation. The variables can be split as

$$\begin{aligned} h(x,y,t) &= \bar{h}(x,y) + h'(x,y,t),\\ u(x,y,t) &= \bar{u}(x,y) + u'(x,y,t),\\ v(x,y,t) &= \bar{v}(x,y) + v'(x,y,t),\\ w_{\mathrm{E}}(x,y,t) &= \bar{w}_{\mathrm{E}}(x,y) + w'_{\mathrm{E}}(x,y,t). \end{aligned}$$

Since the ratio $\frac{h'}{h} = O\left(10^{-2}\right) \ll 1$, momentum terms with h' can be ignored, thus the perturbation equation can be further derived:

$$\underbrace{\frac{\partial}{\partial t}\left(\frac{1}{\Omega}\iint_{\Omega} h'\mathrm{d}S\right)}_{\text{halocline perturbation}} = \underbrace{\frac{1}{\Omega}\oint_{A} h\vec{V}'\cdot\vec{n}\mathrm{d}A}_{\text{advection}} + \underbrace{\frac{1}{\Omega}\iint_{\Omega} -\frac{curl_z\tau'}{\rho_0 f}\mathrm{d}S}_{\text{Ekman pumping}},$$

where $\vec{V}$ is velocity vector; $\vec{n}$ is the normal vector perpendicular to the boundary A; $\rho_0 \approx 1\ 025$ kg/m^3, is the density; $curl_z\tau$ is the vertical component of the ocean surface stress curl; and noting that $w_{\mathrm{E}} = \frac{curl_z\tau}{\rho_0 f}$, is used above. The equation above tells us the halocline perturbation is determined by advection and Ekman pumping.

Figure 10 shows the contribution which the advection term (red line) and the Ekman pumping term (blue line) made to the halocline variations in the simplified model above. The sum (black line in Fig. 10) of the advection term and the Ekman pumping term roughly matches the halocline perturbation from the model output (light blue bars in Fig. 10). Before 2000, the effect of Ekman pumping term is smaller comparing to that of the advection term, that suggests the halocline is controlled by the advection term in this phase. While from 2000 to 2008, the effect of the Ekman pumping term surpasses that of the advection term, thus plays a relatively more important role than the advection term, and dominates the halocline depth variations. In conclusion, the regime of the halocline variations has shifted in the two phases.

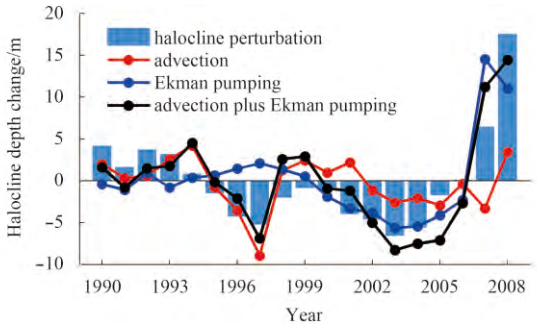

Fig. 10. The halocline depth changes due to advection (red line) and Ekman pumping (blue line). The black line represents the total changes of advection and Ekman pumping that can be compared with the halocline perturbation from the model output denoted by the light blue bars.

We can use the typical upper layer ocean circulation patterns on 50 m in 1997 and 2008 to investigate how the advection term and the Ekman pumping term control halocline variations. Since the sea ice drift can roughly display the ocean circulation on 50 m, Fig. 11 shows that simulation results are in good agreement with ice drift patterns. The model reproduces the weakening of

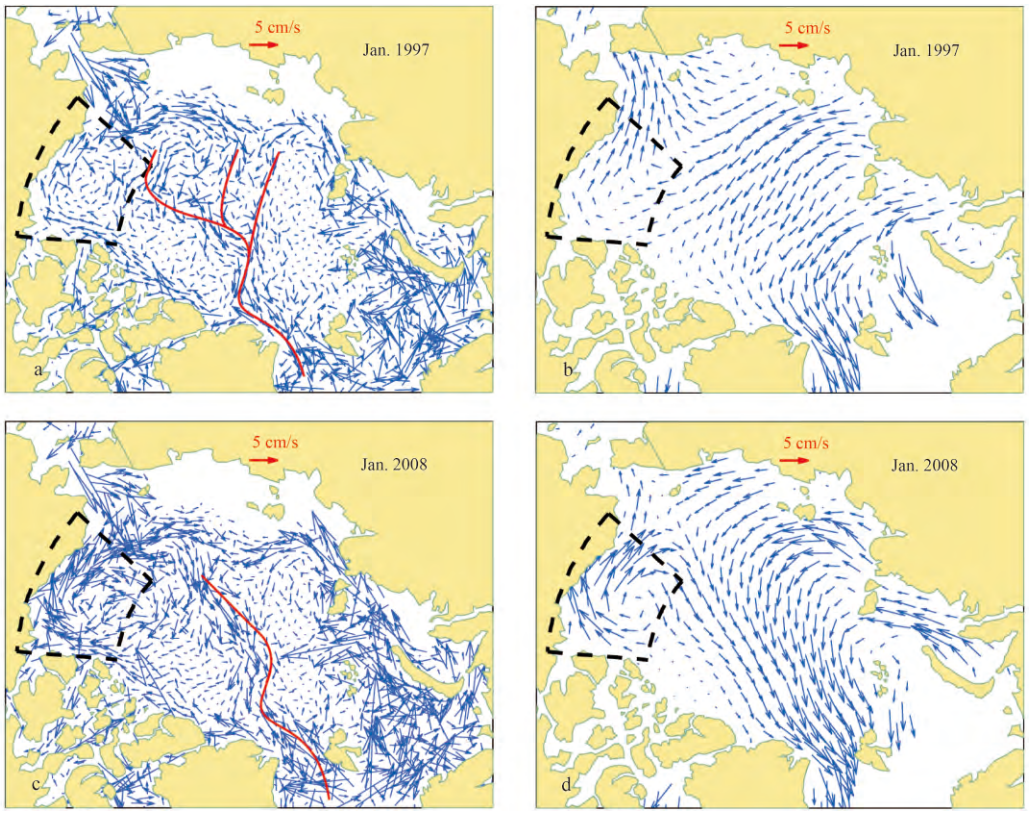

Fig. 11. Simulated ocean current on 50 m (red curves indicate the Transpolar Drift) (a and c) and sea ice motion vector data from the NSIDC (b and d).

the BG in 1997 and strengthening of the BG in 2008 accompanying the Transpolar Drift's pathway spatial transitions. With a branch of the Transpolar Drift entering into the Canada Basin in 1997, the bowl-shaped halocline shrinks in size and towards the Canadian Archipelago (Fig. 3), such that the halocline around the basin is shallowing. As a contrast, the anticyclonic BG controls the whole basin in 2008 with the Transpolar Drift flowing directly to the Fram Strait and the bowl-shaped halocline deepening uniformly. The shift of the Transpolar Drift pathway carries a significant influence on the advection and the Ekman pumping area, further the halocline spatial distribution.

The shift of the Transpolar Drift's pathway is dominated by the spatial deformation of the BH imposed on the Canada Basin. Figure 12 represents that the mean SLP in 1990–1999 (Fig. 12c) is lower than the climatological mean state (Fig. 1), the anomalous low pressure center is located to the north of the Laptev Sea near the North Pole and the center area of the BH is narrow as a strip (Fig. 12a). In 2000–2008, the SLP in the central Arctic Ocean (Fig. 12d) is higher than the climatological mean state (Fig. 1) with anomalous high pressure to the north of the Canadian Archipelago with the broad circular center area of the BH (Fig. 12b). The black dashed lines in Figs 12a and b demonstrate that the BH has an anticyclonic deformation (the black dashed line turns clockwise) in 1990–1999 and the cyclonic deformation (the black dashed line turns counterclockwise) in 2000–2008 relative to the climatological location which indicated by white dashed lines. When the anticyclonic deformation occurs, the geostrophic winds derived from the gradient of SLP are more likely to flow toward the Canada Basin relative to the climatology, so is the Transpolar Drift. In this situation, the Ekman pumping area is shrinking. Also, the strength of the Ekman pumping is weak in this phase. As a result, the halocline depth is dominated by the advection term. On the other hand, when the cyclonic deformation occurs, the geostrophic winds are more likely to flow directly into the Fram Strait. Owing to the area expanding and strengthening of the BH, the Ekman pumping controls the halocline depth in this phase as the previous discussion.

6 Conclusions

Recently, with accelerated melting of sea ice due to rapid warming in the Arctic Ocean, the upper ocean thermohaline structure in the Canada Basin has changed dramatically. The halocline as an essential component dominates the thermodynamic and dynamic processes, such as freshwater content variations in the upper ocean. In this paper, the ice-ocean coupled model is used to study the spatial and temporal variations of the halocline depth in the Canada Basin. Evaluations show the model results are comparable to observations with biases mostly concentrated on the continental slope. Statistical results suggest that the simulation of halocline is reliable.

We then present the time series of the ocean surface stress curl anomaly, the halocline depth, the freshwater content, the upper layer circulation and the intermediate layer circulation in connection to the halocline variations in 1990–2008. The magnitude of the ocean surface stress curl anomaly in 2000–2008 is nearly two times than that in 1990–1999. We hypothesize that with rapid ice melting in recent years, less energy is dissipated by the ice, winds can affect the ocean more efficiently, thus the ocean surface stress curl anomaly variations have changed dramatically. Comparing the simulated results with the SSM/I satel-

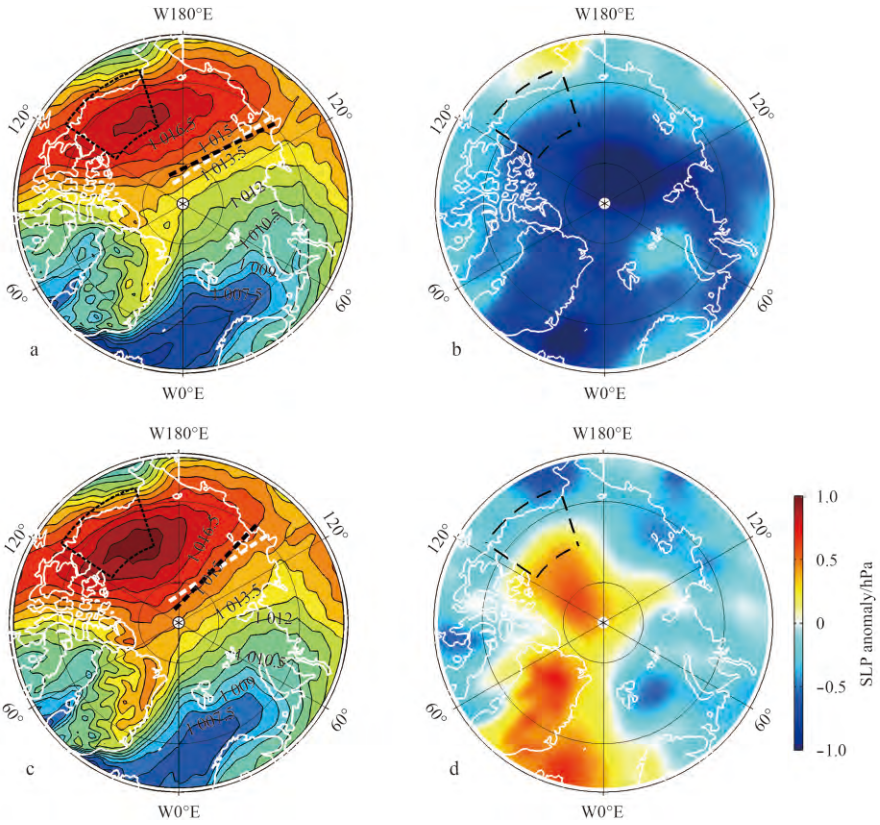

Fig. 12. The mean SLP in 1990–1999 (a), 2000–2008 (b) and the SLP anomaly (c, d) relative to the mean averaged during 1979–2010. The dashed lines in (a, b) are linear fitting of isolines to indicate the BH deformations with white dashed line representing the climatological location in Fig. 1.

lite observations of the September sea ice extent, we find that the two have a consistent interannual variability. More important, both the simulated and observed September ice extent show staircase declines in the two phases, that illustrates the abrupt variations of the ocean surface stress curl anomaly and supports the existence of the simulated variations in reality.

In addition, we find that the seasonal variations of the ocean surface stress curl regulate the Ekman pumping in the Canada Basin, hence dominate seasonal halocline and freshwater variations. On interannual time scale, the variations of the halocline depth have an inverse relationship with the ocean surface stress curl anomaly after 2000, while this relationship is reversed in the 1990s. Response to these changes can also be found in the upper ocean circulation and the intermediate current variations in these two phases. We point out that the regime shift in the Canada Basin is responsible for this phenomena. Specifically, the advection and Ekman pumping dominate the halocline depth variations in turns. According to calculation, the effect of the advection term is more significant than Ekman pumping in 1990–1999, while the dominant term transfers to Ekman pumping in 2000–2008.

Furthermore, the advection and the Ekman pumping are affected by the spatial deformation of BH relative to the climatology which changes the Transpolar Drift's pathway and the Ekman pumping area. In 1990–1999, when the anticyclonic deformation occurs, the Transpolar Drift flows towards the Canada Basin, thus the advection plays a more significant role in controlling the halocline depth. While the cyclonic deformations take places in the 2000s, the Transpolar Drift flows directly to the Fram Strait, the intensity of the Ekman pumping is higher meanwhile, thus regulates the halocline depth in the Canada Basin.

References

Aagaard K, Carmack E C. 1989. The role of sea ice and other fresh water in the arctic circulation. Journal of Geophysical Research: Oceans (1978–2012), 94(C10): 14485–14498

Adcroft A, Campin J M, Hill C, et al. 2004. Implementation of an atmosphere-ocean general circulation model on the expanded spherical cube. Monthly Weather Review, 132(12): 2845–2863

Carmack E C. 2000. The Arctic Ocean's freshwater budget: sources, storage and export. In: Lewis E L, Jones E P, Lemke P, et al., eds. The Freshwater Budget of the Arctic Ocean. Berlin: Springer, 91–126

Carmack E, McLaughlin F, Yamamoto-Kawai M, et al. 2008. Freshwater storage in the northern ocean and the special role of the Beaufort gyre. In: Dickson R R, Meincke J, Rhines P, eds. Arctic-Subarctic Ocean Fluxes. Berlin: Springer, 145–169

Chu P C, Fan Chenwu. 2011. Maximum angle method for determining mixed layer depth from seaglider data. Journal of Oceanography, 67(2): 219–230

Condron A, Winsor P, Hill C, et al. 2009. Simulated response of the arctic freshwater budget to extreme NAO wind forcing. Journal of Climate, 22(9): 2422–2437

Cushman-Roisin, Benoit, 2011. Jean-Marie Beckers. Introduction to Geophysical Fluid Dynamics: Physical and Numerical Aspects. Vol. 101. Academic Press

Daru V, Tenaud C. 2004. High order one-step monotonicity-preserving schemes for unsteady compressible flow calculations. Journal of Computational Physics, 193(2): 563–594

Giles K A, Laxon S W, Ridout A L, et al. 2012. Western Arctic Ocean freshwater storage increased by wind-driven spin-up of the Beaufort gyre. Nature Geoscience, 5(3): 194–197

Heimbach P, Menemenlis D, Losch M, et al. 2010. On the formulation of sea-ice models: Part 2. Lessons from multi-year adjoint sea-ice export sensitivities through the Canadian Arctic Archipelago. Ocean Modelling, 33(1–2): 145–158

Hibler III W D. 1979. A dynamic thermodynamic sea ice model. Journal of Physical Oceanography, 9(4): 815–846

Holloway G. 2008. Observing global ocean topostrophy. Journal of Geophysical Research: Oceans (1978–2012), 113(C7): C07054

Jackett D R, Mcdougall T J. 1995. Minimal adjustment of hydrographic profiles to achieve static stability. Journal of Atmospheric and Oceanic Technology, 12(2): 381–389

Karcher M, Smith J N, Kauker F, et al. 2012. Recent changes in Arctic Ocean circulation revealed by iodine-129 observations and modeling. Journal of Geophysical Research: Oceans (1978–2012), 117(C8): C08007

Lammers R B, Shiklomanov A I, Vörösmarty C J, et al. 2001. Assessment of contemporary arctic river runoff based on observational discharge records. Journal of Geophysical Research: Atmospheres (1984–2012), 106(D4): 3321–3334

Large W G, McWilliams J C, Doney S C. 1994. Oceanic vertical mixing: a review and a model with a nonlocal boundary layer parameterization. Reviews of Geophysics, 32(4): 363–404

Large W G, Pond S. 1982. Sensible and latent heat flux measurements over the ocean. Journal of Physical Oceanography, 12(5): 464–482

Lique C, Johnson H L, Davis P E D. 2015. On the interplay between the circulation in the surface and the intermediate layers of the Arctic Ocean. Journal of Physical Oceanography, 45(5): 1393–1409

Losch M, Menemenlis D, Campin J M, et al. 2010. On the formulation of sea-ice models: Part 1. effects of different solver implementations and parameterizations. Ocean Modelling, 33(1–2): 129–144

Marshall J, Adcroft A, Hill C, et al. 1997. A finite-volume, incompressible Navier Stokes model for studies of the ocean on parallel computers. Journal of Geophysical Research: Oceans, 102(C3): 5753–5766

McLaughlin F A, Carmack E C, Williams W J, et al. 2009. Joint effects of boundary currents and thermohaline intrusions on the warming of Atlantic water in the Canada Basin, 1993–2007. Journal of Geophysical Research: Oceans (1978–2012), 114(C1): C00A12

McPhee M G, Proshutinsky A, Morison J H, et al. 2009. Rapid change in freshwater content of the Arctic Ocean. Geophysical Research Letters, 36(10): L10602

Nguyen A T, Menemenlis D, Kwok R. 2011. Arctic ice-ocean simulation with optimized model parameters: approach and assessment. Journal of Geophysical Research: Oceans (1978–2012), 116(C4): C04025

Nikolopoulos A, Pickart R S, Fratantoni P S, et al. 2009. The western arctic boundary current at 152°W: structure, variability, and transport. Deep Sea Research: Part II. Topical Studies in Oceanography, 56(17): 1164–1181

Onogi K, Tsutsui J, Koide H, et al. 2007. The JRA-25 reanalysis. Journal of the Meteorological Society of Japan, 85(3): 369–432

Proshutinsky A, Krishfield R, Timmermans M L, et al. 2009. Beaufort gyre freshwater reservoir: state and variability from observations. Journal of Geophysical Research: Oceans (1978–2012), 114(C1): C00A10

Rudels B, Friedrich H J, Quadfasel D. 1999. The arctic circumpolar boundary current. Deep Sea Research: Part II. Topical Studies in Oceanography, 46(6–7): 1023–1062

Rudels B, Friedrich H J. 2000. The Transformations of Atlantic Water in the Arctic Ocean and Their Significance for the Freshwater Budget. The Freshwater Budget of the Arctic Ocean,70: 503–532

Shiklomanov I A, Shiklomanov A I, Lammers R B, et al. 2000. The dynamics of river water inflow to the Arctic Ocean. In: Lewis E L, Jones E P, Lemke P, et al., eds. The Freshwater Budget of the Arctic Ocean. Berlin: Springer, 281–296

Shimada K, McLaughlin F, Carmack E, et al. 2004. Penetration of the 1990s warm temperature anomaly of Atlantic water in the Canada Basin. Geophysical Research Letters, 31(20): L20301

Spall M A. 2013. On the circulation of Atlantic water in the Arctic Ocean. Journal of Physical Oceanography, 43(11): 2352–2371

Stewart K D, Haine T W N. 2013. Wind-driven arctic freshwater anomalies. Geophysical Research Letters, 40(23): 6196–6201

Toole J M, Timmermans M L, Perovich D K, et al. Influences of the ocean surface mixed layer and thermohaline stratification on Arctic Sea ice in the central Canada Basin. Journal of Geophysical Research Oceans, 2010, 115(115):234–244.

Washington W M, Semtner Jr A J, Parkinson C, et al. 1976. On the development of a seasonal change sea-ice model. Journal of Physical Oceanography, 6(5): 679–685

Yang Jiayan. 2009. Seasonal and interannual variability of downwelling in the Beaufort Sea. Journal of Geophysical Research: Oceans (1978–2012), 114(C1): C00A14

Zhang Jinlun, Rothrock D A. 2003. Modeling global sea ice with a thickness and enthalpy distribution model in generalized curvilinear coordinates. Monthly Weather Review, 131(5): 845–861

Zhang Jinlun, Steele M. 2007. Effect of vertical mixing on the Atlantic water layer circulation in the Arctic Ocean. Journal of Geophysical Research: Oceans (1978–2012), 112(C4): C04S04